Hindawi
International Journal of Antennas and Propagation
Volume 2021, Article ID 6684959, 14 pages
https://doi.org/10.1155/2021/6684959

Research Article

Design of Window Grille Shape-Based Multiband Antenna for Mobile Terminals

Zhen Yu, Yao Li, Ziheng Lin, and Xiaoying Ran

North China Institute of Science and Technology, Langfang 101601, China

Correspondence should be addressed to Xiaoying Ran; starsky202@ncist.edu.cn

Received 11 December 2020; Revised 8 April 2021; Accepted 27 April 2021; Published 10 May 2021

Academic Editor: Atsushi Mase

Combined with the classic Chinese window grille structure, this paper proposes and designs a multiband microstrip antenna that can be used in wireless mobile terminal equipment. The antenna radiator adopts a rectangular bending structure with four loops, which increases the effective current path of the antenna radiator in a limited space, so that the overall antenna is miniaturized. The branch structure of the four-ring phase set increases the current path of the antenna, making the antenna multiband. The electromagnetic simulation software HFSS was used for antenna modeling and parameter optimization, and the influence of the feed structure, feed mode, and ground plate shape on the antenna was compared and analyzed. The test results show that the antenna can cover four bands, 0.85–1.1 GHz, 1.2–1.8 GHz, 2.40–2.7 GHz, and 5.05–6.3 GHz, and produce 6 main frequency points, 0.9 GHz, 1.3 GHz, 1.6 GHz, 2.55 GHz, 5.3 GHz, and 6.05 GHz. The antenna can cover various navigation systems, Bluetooth, WLAN, ISM frequency band, and 5G (5.725–5.825 GHz).

1. Introduction

With the rapid development of mobile communications and the advent of the 5G era, higher requirements have been placed on the performance of antennas. In recent years, multiband and miniaturized antennas have become the focus of research in mobile terminal equipment. However, due to the inherent narrow-band resonance characteristics of resonant antennas, it is difficult for traditional monopole and dipole antennas to achieve multiband and miniaturized applications in mobile terminals. It can be realized by coupling feeding technology, slot loading technology, matching network loading technology, distributed inductive loading technology, and fractal technology multiband coverage of the antenna. The example corresponds to the following.

Using simple pin short circuit and chip impedance short circuit technology, several high-gain rectangular microstrip patch antennas with different substrates have been designed [1]. Electromagnetic coupling circular patch antenna, with corroded ground, was designed under high frequency [2]. The dual-branch multiband compact slotted antenna, through the introduction of inverted U- and E-shaped branches with different branch lengths and full ground planes, realizes multiple frequency bands [3]. There is a compact slot antenna with offset feed radiation in multiple frequency bands [4]. Multifrequency bands are realized through the coupling between the vertical and horizontal branches at the top.

A dual-frequency rectangular patch antenna that works on 3.5 GHz WiMAX and 5.3 GHz WLAN achieves dual-frequency resonance and miniaturization through two narrow vertical slots [5]. There is a new type of dual-slot loop patch antenna design for multiband applications. Through different slots on the radiator, the current paths are different, and multiband coverage is realized [6]. A small slotted multiband antenna is for wireless applications. The antenna consists of a kite-shaped slot in the radiation patch and C- and G-shaped slots on the ground plane to achieve miniaturization and multiple frequency bands [7]. By adding an improved Minkowski fractal defect ground structure under the center of the radiating patch, the resonant frequency is reduced from 4.16 GHz to 2.4 GHz, and the size is reduced without changing the physical size of the microstrip patch

[8]. By incorporating the "EL" slot into the radiating element together with two identical stubs coupled to part of the ground, the impedance matching and radiation characteristics in the frequency band of interest are improved [9]. A miniaturized antenna is composed of an elliptical ring radiator with three concentric rings and a double T-shaped structure with J-shaped grooves [10].

The matching circuit is designed through the negative impedance converter, transformer, and current buffer, so that the antenna has better impedance matching performance and improves the gain [11].

There is a reconfigurable fractal slot antenna. The frequency reconstruction characteristics are realized by placing the on-off PIN diode on the ground. Multifrequency characteristics are achieved through a slotted ground method combined with a complementary split ring resonator (CSRR) [12]. One is printed on a 1.6 mm thick FR-4 substrate, and the different working modes of the antenna are changed through two switches, and a hp-shaped reconfigurable antenna with six frequency bands is produced [13].

A small notched printed log-periodic dipole array (PLPDA) is based on fractal dipoles. Miniaturization is achieved by applying each dipole element on the curved fractal geometry of PLPDA [14]. By imitating the branch and fractal structure of trees, the current path and the electrical length of the antenna are increased, so that the antenna generates multiple frequency bands [15]. A multiband, high-gain, miniaturized fractal microstrip antenna is suitable for modern communication systems [16].

Compared with the antennas in the above-mentioned references, the window grille antenna has a simpler and controllable structure. By simply bending the branches, the antenna as a whole becomes compact. In addition, the combination of antenna and grid makes the antenna design more artistic. Finally, the designed antenna does not add any auxiliary circuit and can also meet more than ten communication performance indicators.

At present, the research on new antenna technology at home and abroad has initially matured, and certain theories and methods have been formed. All kinds of pane patterns, complex and changeable shapes and structures, have important research value for antenna design and the realization of miniaturized multiband technology. This article starts from the cross structure in the basic structure of Chinese classical grilles. The cross structure has good support strength in the window panes, and the overall amount of daylighting is also good. It is often used in the classical window grill culture. In this antenna design, the cross structure means that the two monopoles are orthogonal to produce dual polarization. The four sides are extended and bent, and finally a rectangular bent structure with four rings is formed, which greatly reduces the overall size of the antenna. At the same time, the current path on the surface of the antenna radiator is increased to make the antenna meet the requirements of miniaturization and multiband. The line width of the antenna radiator is 2 mm. If the length is not bent, the side length will reach 128 mm, and the coverage area of the radiator will reach $128 \times 128\ \text{mm}^2$. After bending and folding, the side length of the radiator remains unchanged, but the overall radiator area is reduced to $50 \times 24 \times 2\ \text{mm}^2$-$24 \times 24\ \text{mm}^2$. The spatial variation of the antenna radiator is shown in Figure 1.

1.1. Antenna Parameter Theory and Classical Grille Structure. The calculation formulas for the antenna microstrip line width and antenna electrical length used in the article are as follows.

1.1.1. Antenna Feeder Width.

$$W = \frac{c}{2f_r}\left(\frac{\varepsilon_r + 1}{2}\right)^{-(1/2)}. \quad (1)$$

Here, W is the width of the antenna feeder, c is the speed of light in free space, f_r is the central frequency of the antenna's work, and ε_r is the dielectric constant of the antenna's dielectric material.

1.1.2. Antenna Length.

$$L = \frac{\lambda_g}{2} - 2\Delta l = \frac{c}{2f_r\sqrt{\varepsilon_e}} - 2\Delta l. \quad (2)$$

Here, Δl is the antenna length correction amount and ε_e is the effective dielectric constant of the antenna. According to the obtained length and width of the antenna, and the parameters of the antenna dielectric plate, the approximate size of the antenna can be designed, and through software simulation analysis, the antenna can meet the design requirements.

1.1.3. Classical Grille Structure. The grilles are all selected of suitable patterns. The grilles in Shandong are mostly straight, which is suitable for the mullioned windows in the area. The window grilles in the northwest divide the complete papercut into four pieces with the word "ten" in Fengzhong, which is also suitable for the formation of a cross grid in the center of the window. This antenna combines classical window grille structure with modern antenna theory. It starts with a classical window grille-based cross structure with four sides extended. In order to control the size of the space, it is folded three times to form a rectangular four-loop structure. The whole looks like it is rotating in one direction, which is similar to the Tai Chi spiral pattern in traditional Chinese culture. The structure is simple, and more branches help to achieve multiple frequency bands. The classical window grille cross structure is shown in Figure 2.

2. Antenna Structure and Design Procedure

2.1. Design and Structure of Window Grille-Shaped Antenna. The antenna imitates the classical window grille cross-structure antenna. By changing the direction of the cross structure and the feeding mode, the current flow direction of the radiator and the length of the current path are changed, thereby achieving multiband coverage. Among them, the

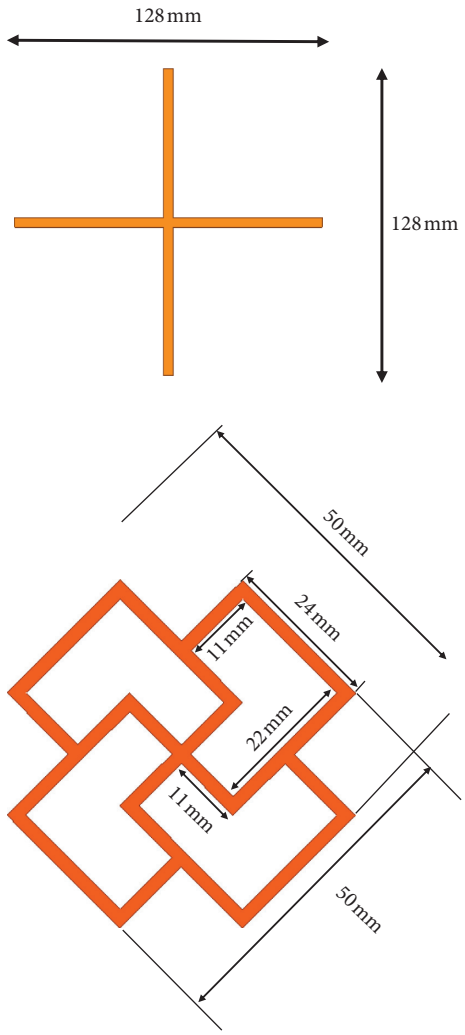

Figure 1: Spatial variation of the antenna radiator.

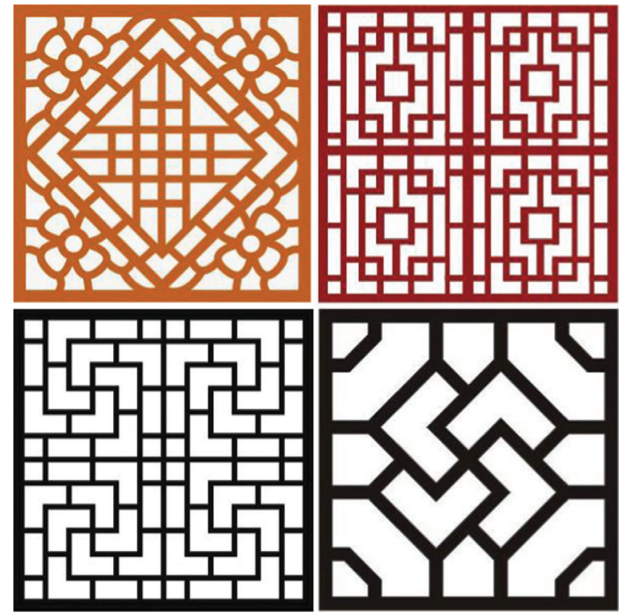

Figure 2: Classical window grille cross structure.

Table 1: Antenna parameters.

X1	Y1	Gnd_X	H	H2	H3	H4
95 mm	55 mm	30 mm	65 mm	26 mm	2 mm	5 mm
L	L1	L2	W	W1	W2	h
24 mm	19 mm	32 mm	2 mm	1 mm	1 mm	1.6 mm

bifurcated feed structure adopted by the feed mode [19] is conducive to improve the radiation performance and efficiency of the antenna. The antenna uses a polytetrafluoroethylene glass cloth plate (FR4) with a dielectric constant $\varepsilon r = 4.4$, a thickness $h = 1.6$ mm, and a dielectric loss tangent $\tan\delta = 0.02$ as the antenna dielectric body, and a 50 Ω microstrip line feeder structure. The overall size of the antenna is $95 \times 55 \times 1.6\,\text{mm}^3$, and the structure and size parameters of the antenna are shown in Table 1 and Figure 3. The upper surface is the antenna radiator, the back is the ground plate, and the middle is the dielectric plate.

The width of the antenna feed line, the center frequency fc = 2.4 GHz, and the dielectric constant $\varepsilon r = 4.4$ of the dielectric plate are calculated by formula (1), and the antenna feed line width $w1 = 1$ mm.

The antenna radiator generation process is shown in Figure 4. A cross structure with a width of 2 mm and a length of 11 mm on each side is shown in Figure 4(a). Figure 4(b) is on the basis of Figure 4(a). The end of the branch is rotated 90° counterclockwise to produce a new branch with a length of 22 mm and the width remains the same. Figure 4(c) is bent 90° counterclockwise at the end of the branch in Figure 4(b) to produce a new branch of 24 mm. Finally, in Figure 4(d), at the end of the branch in Figure 4(c), bend a branch with a length of 11 mm by 90° counterclockwise to form a rectangular four-ring closed phase sleeve structure as a whole.

2.2. Parameter Optimization. The basic model of the antenna is a crisscross stub microstrip antenna with a microstrip line and a rectangular ground structure, as shown in Figure 5. In the final model, the bifurcated feed structure is adopted to enhance the current input, and the width is 1 mm, which achieves good matching with the 50 Ω feeder and expands the bandwidth. The tortuous branches of the classical window grille cross structure increase the current path, and it is easy to realize the multiband of the antenna. After simulation, the antenna under this structure has five central resonance frequencies of 1.45 GHz, 2.45 GHz, 3.85 GHz, 5.13 GHz, and 5.8 GHz, and their frequencies are about 1.5 times, 2.5 times, 4 times, 5.5 times, and 0.9 GHz, respectively, 6.5 times the relationship. The return loss comparison between the basic model and the final model is shown in Figure 6. Compared with the unrotated basic model, the final model produced two new 5G communication frequency points, 5.13 GHz and 5.8 GHz, with bandwidths of 4.79–5.37 GHz and 5.6–5.99 GHz, respectively, in line with the antenna multiband design concept.

The comparison diagram when the antenna feed structure is bident and trident is shown in Figure 7, and the

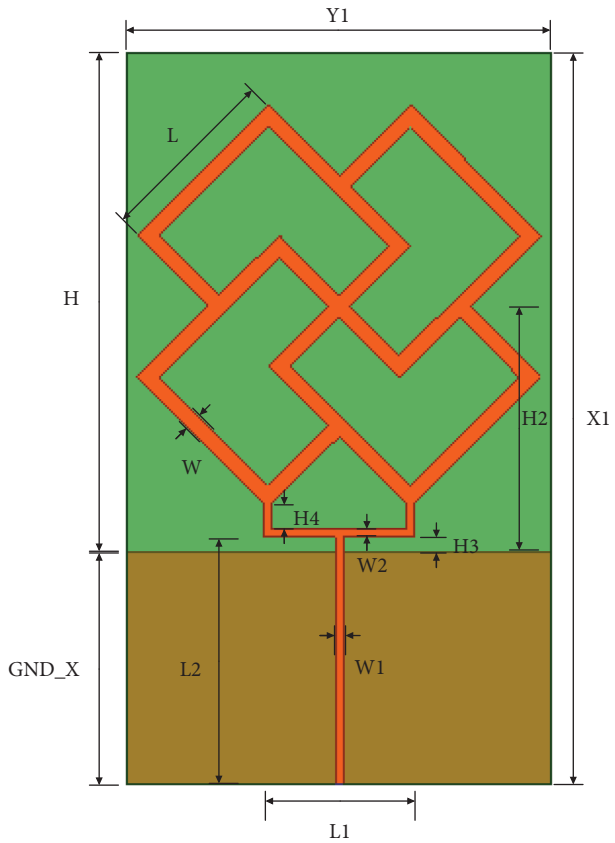

Figure 3: Imitating the classical window grille cross-structure antenna model structure.

Figure 4: Diagram of the antenna radiator generation process.

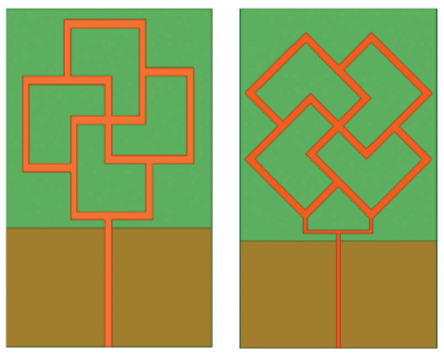

Figure 5: Model comparison. (a) Basic model. (b) Final model.

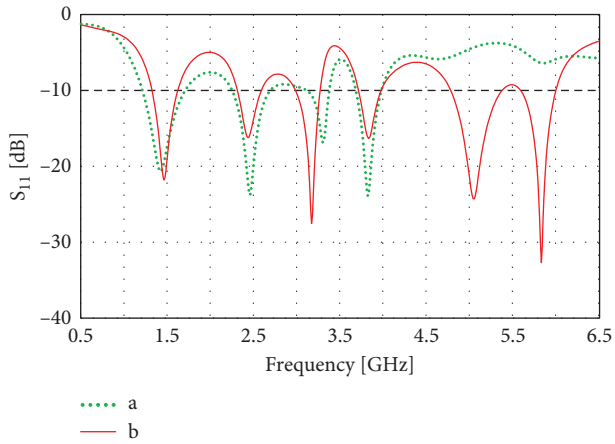

Figure 6: Comparison of the basic model and final model.

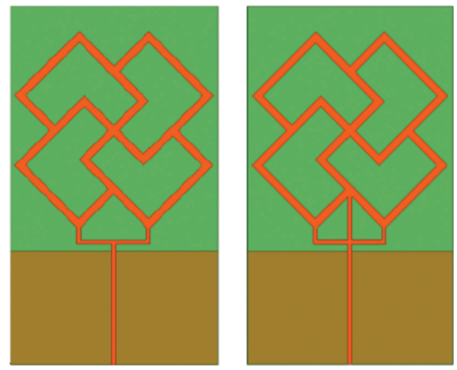

Figure 7: Comparison of microstrip line feed structure. (a) Double-dent structure. (b) Trident structure.

return loss comparison in the corresponding situation is shown in Figure 8.

Compared with the antenna simulation result under the trident structure feeder, the antenna simulation result under the double-dent structure feeder has one more usable frequency point of 5.8 GHz in the high frequency part, and the return loss value reaches 22.32 dBi. In the low frequency part, the frequency point of the antenna simulation result under the trident structure is shifted, which is 2.56 GHz at the 2.45 frequency point, and the shift amount is 0.11 GHz. At the frequency point of 5.13 GHz, the antenna frequency point under the trident feeder structure is shifted to 5.02 GHz, and the shift amount is 0.11 GHz. At the same time, the simulation result of the antenna return loss under the double-dent feeder structure is below -10 dB. The bandwidth is wider and the range is 4.9–5.35 GHz. The antenna range under the trident structure is 4.85–5.21 GHz, as shown in Figure 8. Therefore, the double-dent feeder structure is more suitable for the antenna than the trident feeder structure.

The antenna feeding method is divided into a microstrip line structure and a coplanar waveguide structure. As shown in Figure 9. The return loss comparison of the two feeding modes is shown in Figure 10. At frequencies before 2 GHz,

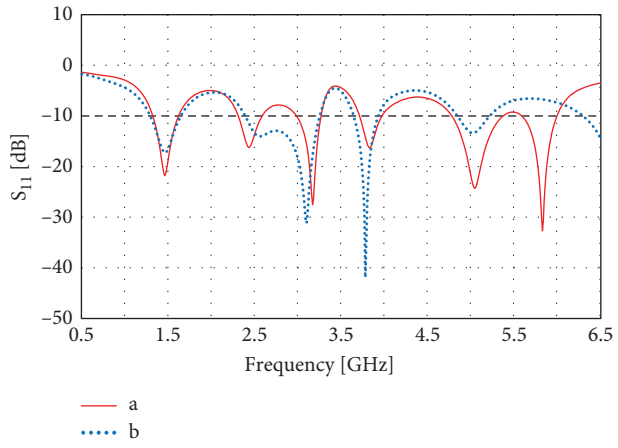

Figure 8: Comparison of antenna return loss between double-dent structure and trident structure.

the resonant frequency under the coplanar waveguide structure model antenna moves 0.7 GHz to the left compared to the resonant frequency of the microstrip line structure model antenna, while at the resonant frequency after 2 GHz, the latter shifts to the right as a whole. The offset is 0.2 GHz, 0.15 GHz, 0.15 GHz, 0.3 GHz, and 0.4 GHz.

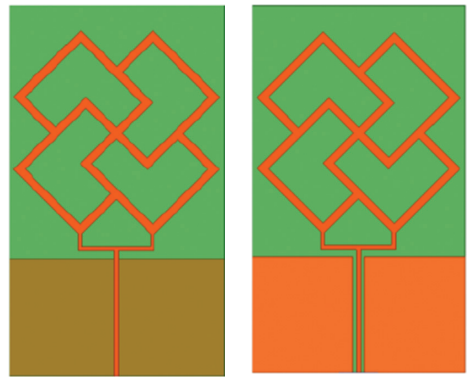

Figure 9: Comparison of power feeding methods. (a) Microstrip line structure. (b) Coplanar waveguide structure.

Therefore, the resonance frequency band corresponding to the resonance frequency point of the antenna under the coplanar waveguide structure is not completely covered by the available communication frequency band. The center resonance frequency point generated by the microstrip line structure model is closer to the common communication frequency point, and the bandwidth is wider, and the overall return loss performance is also better. Figure 10. Therefore, the feed mode of the microstrip line structure is more suitable for imitating the classical grille cross-structure antenna.

The model is a rectangular ground plate; Figure 11(b) model is a trapezoidal ground structure formed by cutting two right angles above the ground plate on the basis of Figure 11(a) model; the ground plate of Figure 11(c) is rectangular ground plane; the comparison of antenna return loss under various ground shapes is shown in Figure 12; the antenna has produced a total of five usable resonance frequencies of 1.45 GHz, 2.45 GHz, 3.86 GHz, 5.13 GHz, and 5.85 GHz. The trapezoidal ground plate antenna produced a total of four usable resonance frequencies of 1.42 GHz, 2.4 GHz, 5.05 GHz, and 5.86 GHz. The elliptical ground plate antenna produced a total of five available resonant frequencies of 1.46 GHz, 2.39 GHz, 3.82 GHz, 5.06 GHz, and 5.9 GHz. By comparing the three return loss diagrams, the model has an available frequency of 3.86 GHz, more than model *b*, and the return loss value is −15.44 dB. In the return loss curve of the antenna model, the center frequency is closer to the common communication frequency than in the *c* model, and the isolation is stronger. In comprehensive comparison, the rectangular ground plate is more suitable for this antenna.

2.3. Simulation Results. The S11 return loss curve of the final shaped antenna is shown in Figure 13. The five available center resonance frequencies are 1.45 GHz, 2.45 GHz, 3.85 GHz, 5.13 GHz, and 5.8 GHz, and the reflection losses are -23.44 dB, -16.01 dB, -17.38 dB, -23.47 dB, and -29.42 dB, respectively. Bandwidth under -10 dB is 1.31–1.63 GHz (22.1%), which can cover GPS (1.575–1.625 GHz), TD-LTE (B-TrunC) (1.447–1.467 GHz). 2.31–2.57 GHz (10.6%) can cover Bluetooth

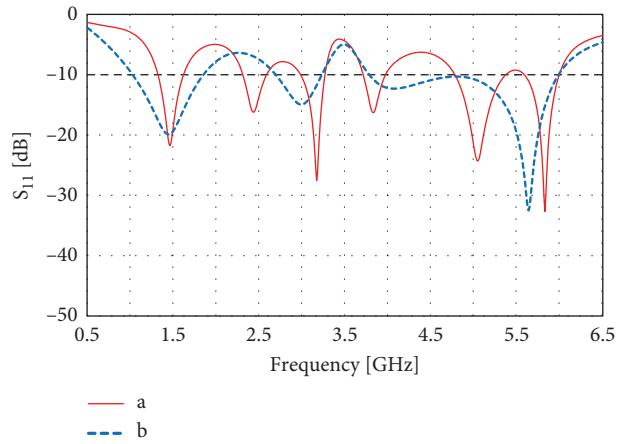

Figure 10: Comparison of microstrip line structure and coplanar waveguide structure.

(2.4–2.485 GHz), WLAN (2.4–2.4835 GHz), LTE Band40 (2300–2400 MHz), ISM Band (2.420–2.4835 GHz), WiMAX (2.3 GHz), and WLAN (802.11 b/g/*n*:2.4–2.48 GHz). 3.71–4.05 GHz (8.8%) can cover LTE42/43 (3.4–3.8 GHz) and WiMAX (3.3–3.8 GHz). 4.81–5.40 GHz(11.6%) can cover WLAN (802.11a/*n*:5.15–5.35 GHz); 5.60–6.02 GHz (7.2%) can cover 5G (5.725–5.825 GHz) and other wireless communication systems, as shown in Table 2.

2.4. Current Distribution on the Antenna Surface. The surface current amplitude and vector distribution of the antenna are at the center resonant frequencies of 1.45 GHz, 2.45 GHz, 3.85 GHz, 5.13 GHz, and 5.80 GHz (Figure 14).

When the length of the antenna is 1/4 the wavelength of the radio signal, the transmission and reception conversion efficiency of the antenna is at its highest. Therefore, the length of the antenna will be determined according to the frequency or wavelength of the transmitted and received signals.

Through calculation, the ideal antenna length at each frequency point is 5.2 cm, 3.1 cm, 1.9 cm, 1.5 cm, and 1.3 cm, respectively. Observing the size of the antenna and calculating it, it can be concluded that the internal branches

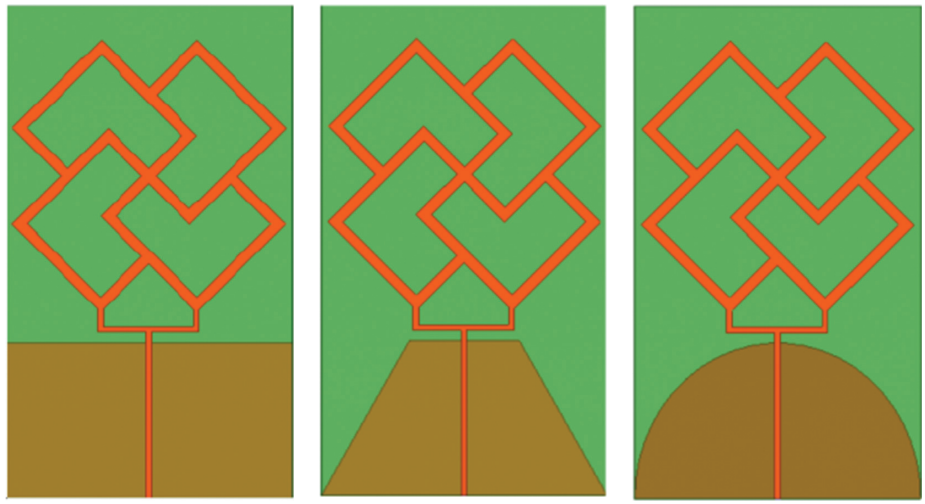

Figure 11: Comparison of ground plates. (a) Rectangular ground. (b) Trapezoidal ground. (c) Oval ground.

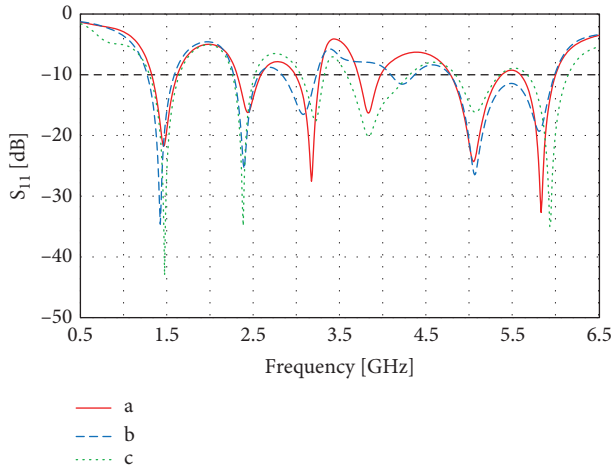

Figure 12: Comparison of return loss under different shapes of ground plates.

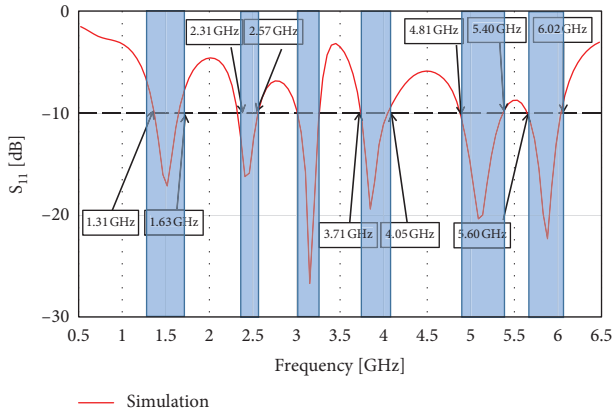

Figure 13: The return loss of a multiband microstrip antenna with a cross-structure imitation classical grille.

Table 2: Antenna coverage frequency band.

Frequency band	Covered communication frequency band
1.31–1.63 GHz (22.1%)	GPS (1.575–1.625 GHz) TD-LTE (B-trunc) (1.447–1.467 GHz)
2.31–2.57 GHz (10.6%)	Bluetooth (2.4–2.485 GHz) WLAN (2.4–2.4835 GHz) LTE Band40 (2300–2400 MHz) ISM Band (2.420–2.4835 GHz) WiMAX (2.3 GHz) WLAN (802.11 b/g/*n*:2.4–2.48 GHz)
3.71–4.05 GHz (8.8%)	LTE42/43 (3.4–3.8 GHz) WiMAX (3.3–3.8 GHz)
4.81–5.40 GHz (11.6%)	WLAN (802.11a/*n*:5.15–5.35 GHz)
5.60–6.02 GHz (7.2%)	5G (5.725–5.825 GHz)

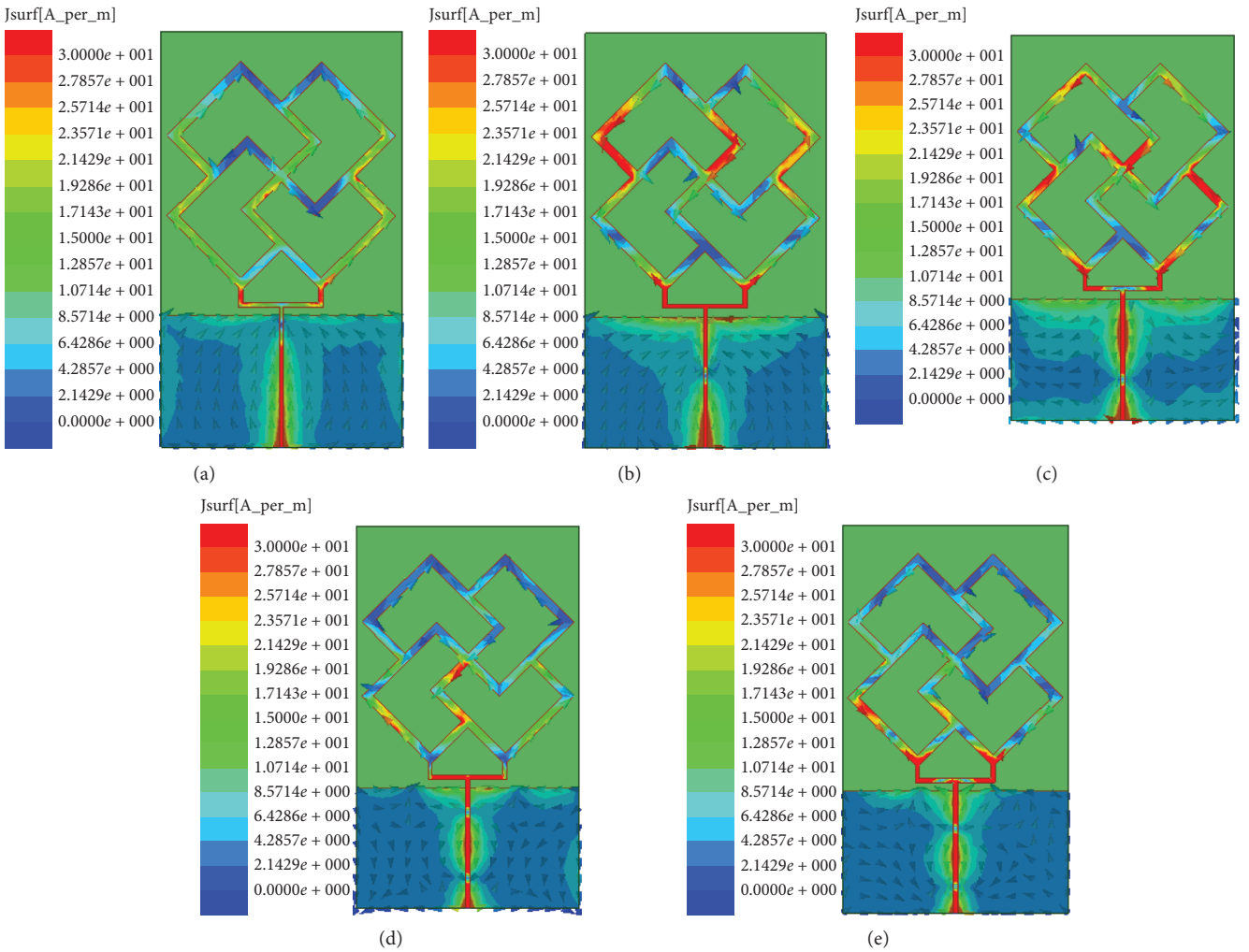

Figure 14: The current amplitude and vector distribution on the surface of a microstrip antenna with a cross structure imitating classical grilles: (a) 1.45 GHz, (b) 2.45 GHz, (c) 3.85 GHz, (d) 5.13 GHz, and (e) 5.80 GHz.

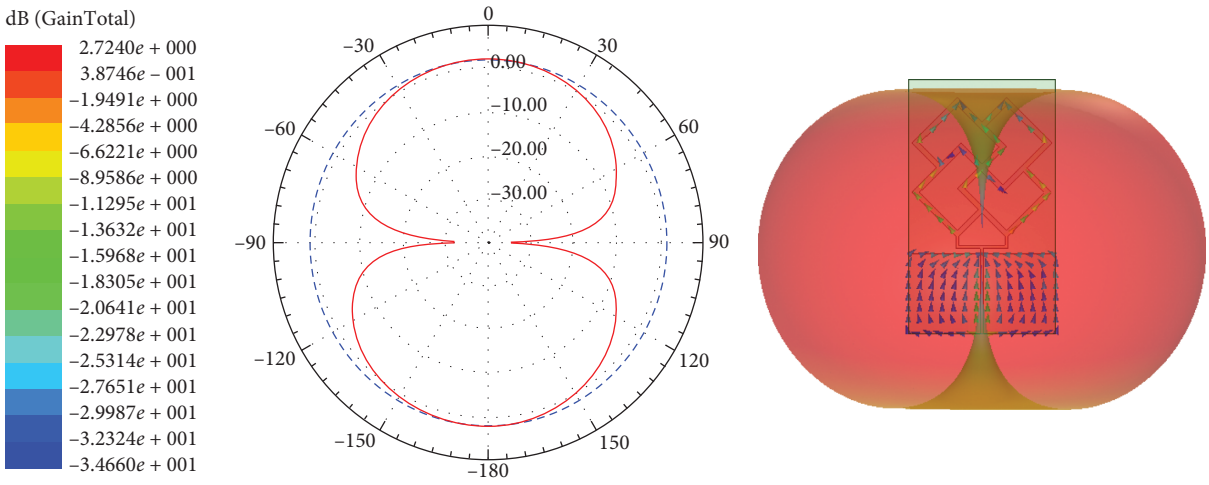

(a)

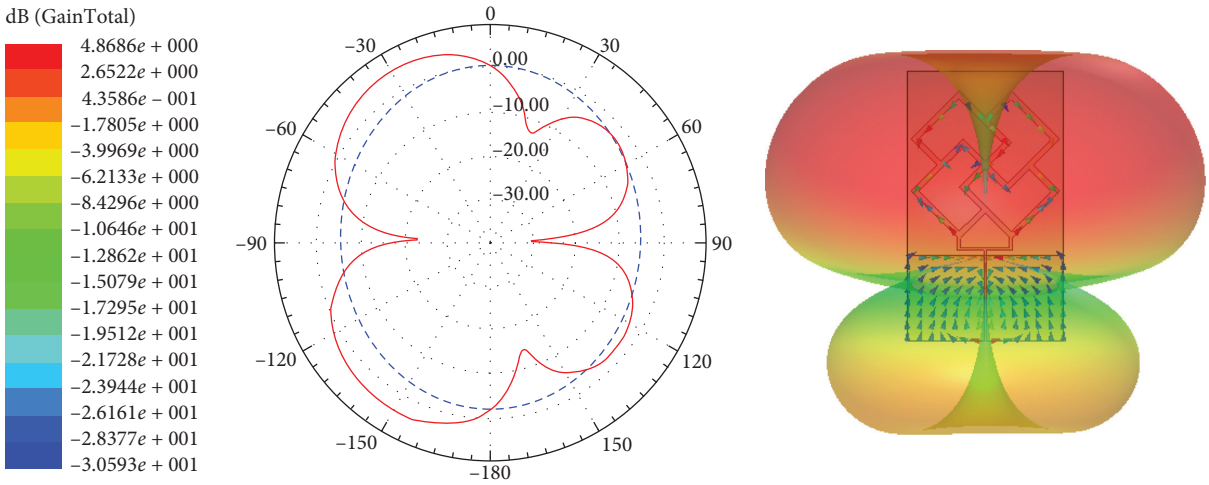

(b)

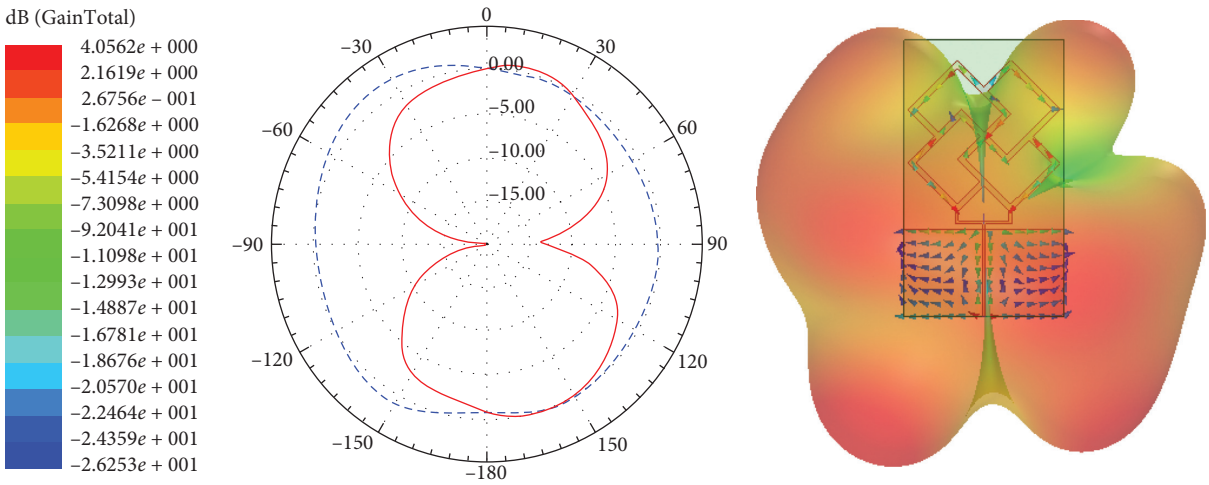

(c)

Figure 15: Continued.

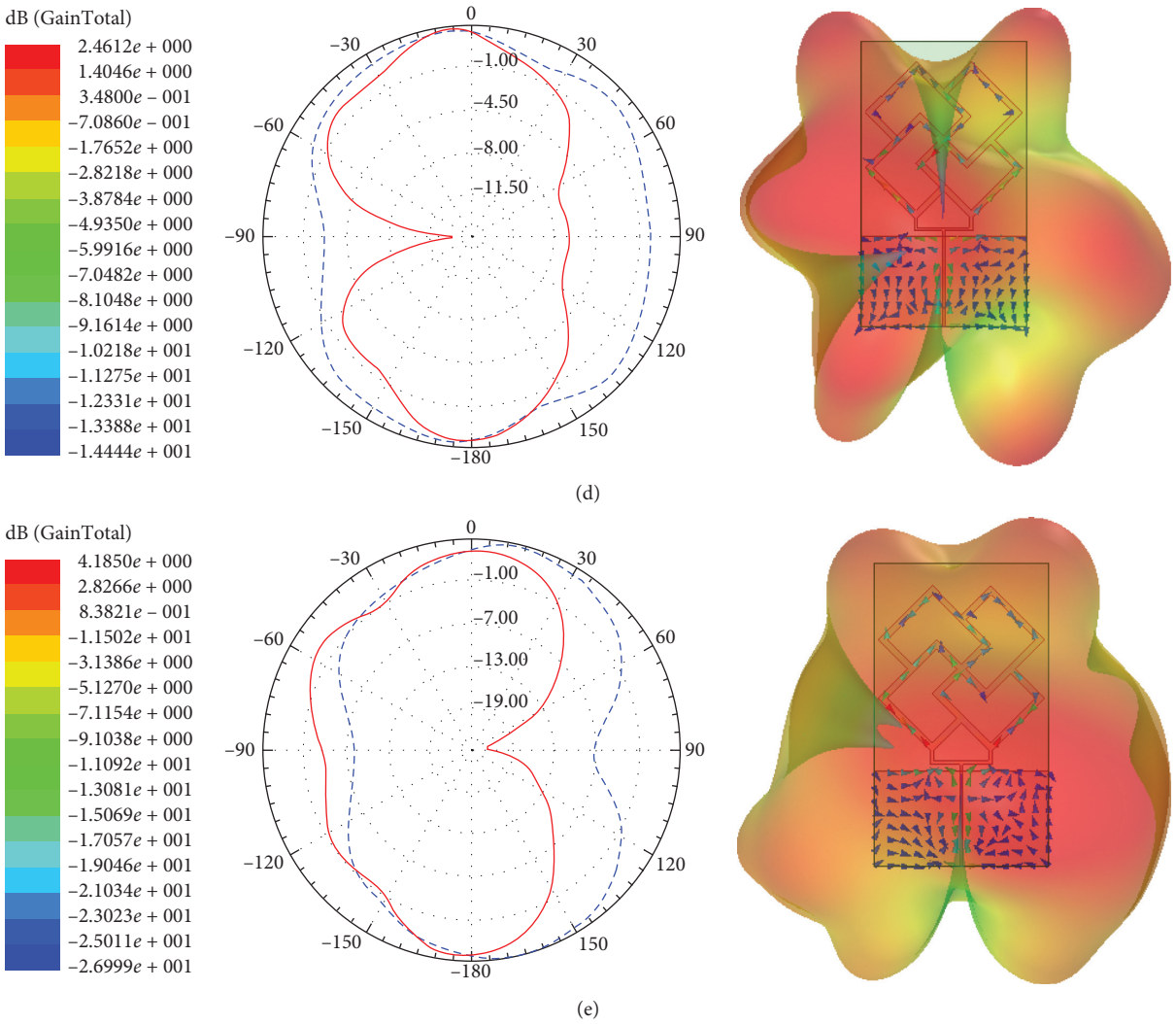

Figure 15: Pattern gain and E/H pattern of a microstrip antenna with a cross structure imitating classical grilles. (a) 1.45 GHz, (b) 2.45 GHz, (c) 3.85 GHz, (d) 5.13 GHz, and (e) 5.80 GHz.

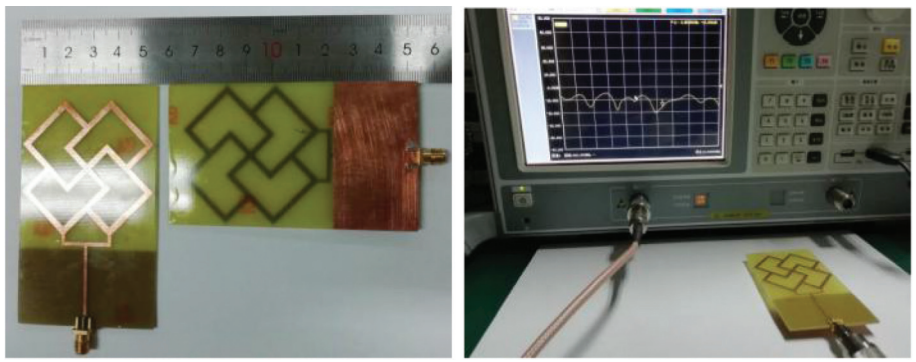

Figure 16: The prototype of a microstrip antenna with a cross structure imitating classical grilles and a vector network analyzer test device.

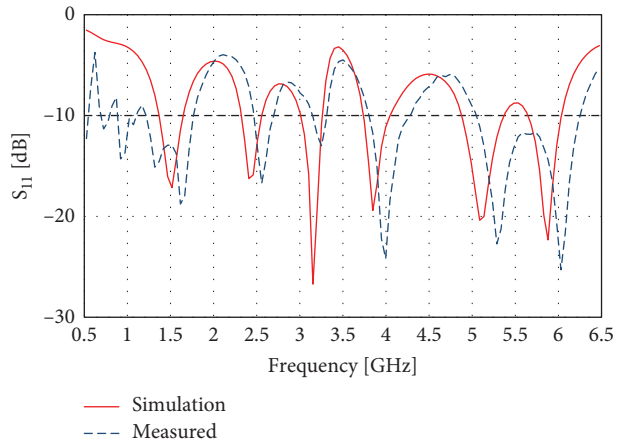

Figure 17: Antenna measured value and simulated value comparison.

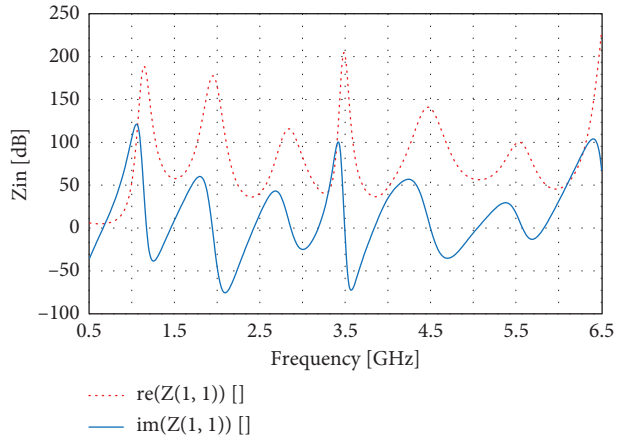

Figure 18: The graph of Z_{in} versus frequency.

Table 3: Antenna measured frequency band coverage.

Frequency band	Bandwidth	Commercial frequency band coverage
1	0.85–1.1 GHz (27.8%)	GSM900 (800–960 MHz)
2	1.2–1.75 GHz (37.9%)	GPS (1.575–1.625 GHz) TD-lte (B-TrunC) (1.447–1.467 GHz) GLONASS (L1, L2) BD2 (B1, B2, B3)
3	2.45–2.7 GHz (9.8%)	WLAN (802.11 b/g/*n*:2.4–2.48 GHz) Bluetooth (2.4–2.485 GHz) WLAN (2.4–2.4835 GHz) ISM Band (2.420–2.4835 GHz)
4	5.05–6.30323 GHz (21.7%)	WLAN(802.11a/*n*:5.15–5.35 GHz, 5.725–5.850 GHz) 5G (5.725–5.825 GHz)

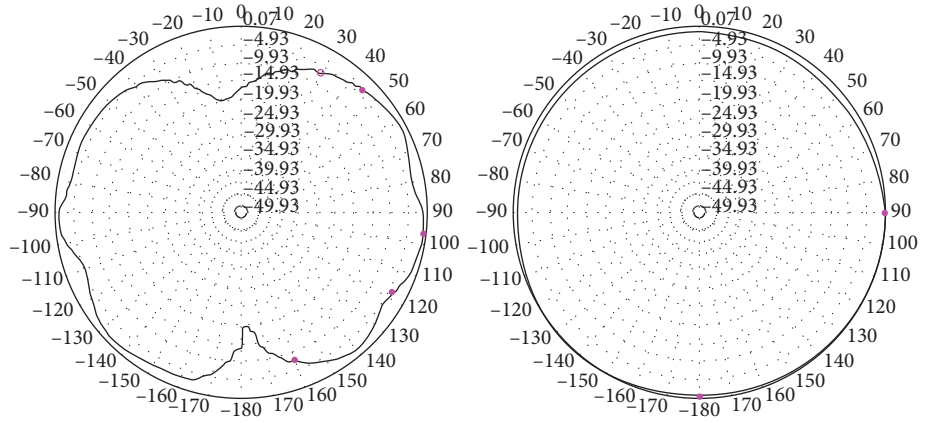

(a)

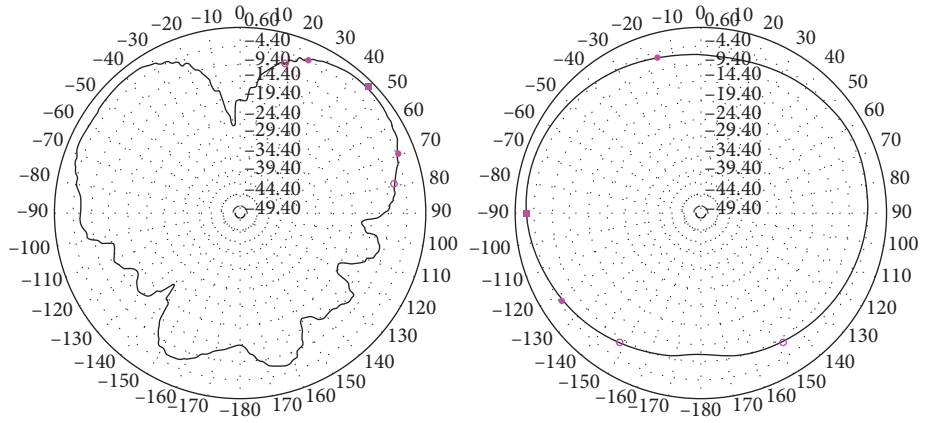

(b)

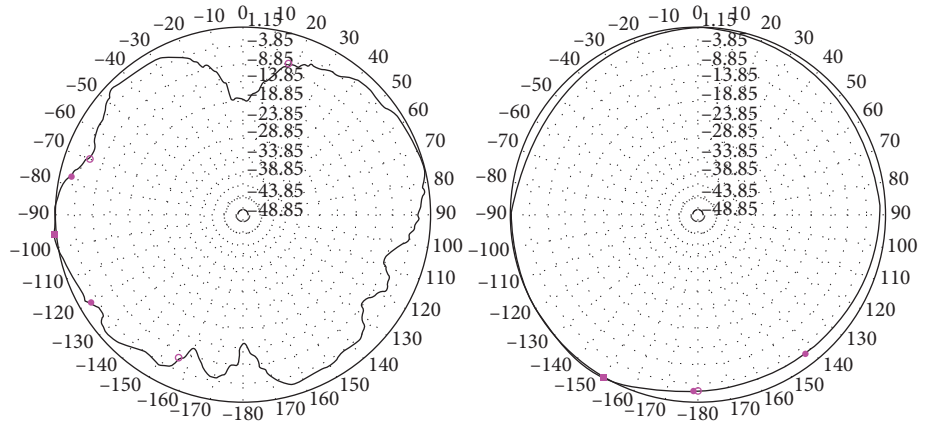

(c)

Figure 19: Continued.

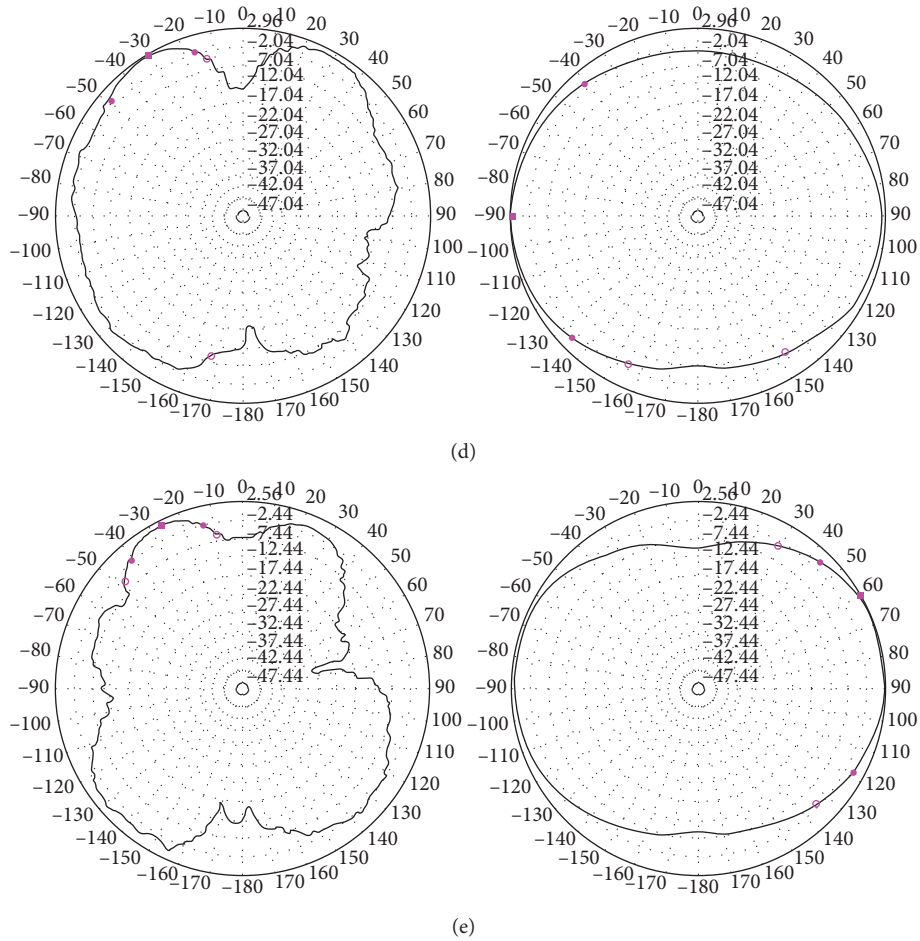

Figure 19: E/H pattern. (a) 1.45 GHz, (b) 2.45 GHz, (c) 3.85 GHz, (d) 5.13 GHz, and (e) 5.80 GHz.

formed by the classical grille cross structure can make the current path flowing through the antenna surface longer. The actual current path length at each frequency point is 5.82 cm, 5.22 cm, 4.06 cm, 2.74 cm, and 1.77 cm. From the above figure, *c* for the antenna radiator at low resonance frequency, there is more current distribution at the edge of the branch. As the operating frequency increases, the current gradually shifts to the bottom of the antenna, and the current intensity at the edge of the branch increases.

2.5. Antenna Gain and Directional Characteristics. The center resonance frequencies are 1.45 GHz, 2.45 GHz, 3.85 GHz, and 5.1 GHz, and the simulated E/H pattern and simulated 3D gain were at 5.8 GHz (the red solid line represents the E-plane pattern, and the blue dashed line represents the H-plane pattern) (Figure 15). The E-plane and H-plane of the antenna have good omnidirectional radiation characteristics in the low frequency band.

In the low frequency band, the antenna has better omnidirectional radiation characteristics; as the frequency increases, more side lobe levels and side lobes appear in the pattern. In the entire working frequency range of the antenna, the antenna maintains good radiation characteristics, and there is no zero point.

3. Fabrication and Measured Results

3.1. Test Results and Performance Analysis. The front and back view of the multiband imitation classical window grille cross-structure microstrip antenna are shown in Figure 16**.** The antenna dielectric substrate is a 1.6 mm thick G10/FR4 dielectric plate, and the antenna metal radiator and ground plate are 30 μm thick metal copper. Use Agilent vector network analyzer N5230 C to test the impedance and direction characteristics of the antenna.

Compare the measured return loss with the simulation results, as shown in Figure 17. It can be seen that the center resonant frequency of the antenna has shifted from the −10 dB bandwidth, and the antenna test bandwidth matches the simulation bandwidth and maintains good consistency overall.

The relationship between Zin and the final design frequency is shown in Figure 18.

It can be seen from the test curve that the antenna −10 dB bandwidth is 0.85–1.1 GHz (27.8%), 1.2–1.75 GHz (37.9%), 2.45–2.70 GHz (9.8%), and 5.05–6.3 GHz (21.7%). The communication frequency bands that these frequency bands can cover are consistent with the simulation results, as shown in Table 3.

The measured EH surface radiation pattern of the antenna is shown in Figure 19.

4. Conclusion

The antenna adopts an imitated classical window grille cross structure, and its own zigzag branches increase the current path of the antenna and increase the resonance frequency. The closed structure formed by the crisscross forms a circular radiator. Then use the dual-dent power feeding method to make 50 Ω impedance matching easier, and the overall size of the antenna is $95 \times 55 \times 1.6\,mm^3$. The antenna test results are in good agreement with the simulation results, verifying the rationality of the design. The antenna has good omnidirectional radiation characteristics, and the four working frequency bands are 0.85–1.1 GHz, 1.2–1.8 GHz, 2.45–2.7 GHz, and 5.05–6.3 GHz, which can meet the requirements of a variety of mobile.

Data Availability

The simulation and test data used to support the findings of this study are included within the article.

Conflicts of Interest

The authors declare that they have no conflicts of interest.

Acknowledgments

This work was supported in part by the National Natural Science Foundation of China (no. 61663014), National Key R&D Project (no. 2020YFC1511805), Hebei Higher Education Teaching Reform Project under Grant 2018GJJG477, Fundamental Research Funds for the Central Universities under Grant nos. 3142018047 and 3142018048, and Project of Hebei Higher Education Association under Grant GJXH2015-1332.

References

[1] A. Narayan, B. B. Mangaraj, G. P. Mishra, and R. Pathak, "An improved compact antenna design proposed for 5G cellular band," *International Journal of Sensors, Wireless Communications and Control*, vol. 10, no. 6, 2020.

[2] A. B. Sahoo and B. B. Mangaraj, "A miniaturized electromagnetically coupled patch antenna design using eroded ground plane," *Microwave and Optical Technology Letters*, vol. 62, no. 11, 2020.

[3] A. Desai, R. Patel, T. Upadhyaya, H. Kaushal, and V. Dhasarathan, "Multiband inverted E and U shaped compact antenna for Digital broadcasting, wireless, and sub 6 GHz 5G applications," *AEU-International Journal of Electronics and Communications*, vol. 123, Article ID 153296, 2020.

[4] R. Patel, A. Desai, T. Upadhyaya et al., "Meandered low profile multiband antenna for wireless communication applications," *Wireless Networks*, vol. 27, no. 8, 2021.

[5] A. B. Sahoo, G. P. Mishra, and B. B. Mangaraj, "Optimal design of compact dual-band slot antenna using particle swarm optimization for WLAN and WiMAX applications," *Recent Advances in Electrical & Electronic Engineering (Formerly Recent Patents on Electrical & Electronic Engineering)*, vol. 11, 2019.

[6] A. B. Sahoo, G. P. Mishra, and B. B. Mangaraj, "A novel dual slot circular patch antenna design for multi-band applications," *Microwave Review*, vol. 24, 2018.

[7] T. Ali, K. D. Prasad, and R. C. Biradar, "A miniaturized slotted multiband antenna for wireless applications," *Journal of Computational Electronics*, vol. 17, no. 2, 2018.

[8] G. P. Mishra and B. B. Mangaraj, "Highly compact microstrip patch design based on improved capacitive Minkowski fractal defected ground structure," *AEUE-International Journal of Electronics and Communications*, vol. 115, 2020.

[9] J. Kulkarni, A. Desai, and C.-Y. D. Sim, "Wideband Four-Port MIMO antenna array with high isolation for future wireless systems," *AEU-International Journal of Electronics and Communications*, vol. 128, Article ID 153507, 2021.

[10] J. Kulkarni and C.-Y.-D. Sim, "Wideband cpw-fed oval-shaped monopole antenna for wi-fi5 and wi-fi6 applications," *Progress In Electromagnetics Research C*, vol. 107, pp. 173–182, 2021.

[11] Yi Ren, De Huang, F. Baoxin, Q. Ren, H. Hu, and J. Zhou, "A high gain, compact active disc-cone antenna based on non-foster matching circuit," *AEU-International Journal of Electronics and Co mmunications*, vol. 133, 2021.

[12] A. Tanweer, F. Nikhat, and R. C. Biradar, "A miniaturized multiband reconfigurable fractal slot antenna for GPS/GNSS/Bluetooth/WiMAX/X-band Applications," *AEU-International Journal of Electronics and Communications*, vol. 94, pp. 234–243, 2018.

[13] S. Ullah, S. Ahmad, B. A. Khan, F. A. Tahir, and J. A. Flint, "An hp-shape hexa-band antenna for multi-standard wireless co mmunication systems," *Springer US*, vol. 25, no. 3, 2019.

[14] M. R. Jena, S. Sahoo, G. P. Mishra et al., "Miniaturized band notched printed LPDA design with meander fractal dipole for UWB communication," *International Journal of Electronics*, vol. 108, 2020.

[15] X. Ran, Z. Yu, T. Xie, L. Yao, X. Wang, and P. Huang, "A novel dual-band binary branch fractal bionic antenna for mobile terminals," *International Journal of Antennas and Propagation*, vol. 2020, Article ID 6109093, 9 pages, 2020.

[16] D. Tiwari, J. A. Ansari, and K. Abhishek, "Analysis of a miniaturized hexagonal sierpinski gasket fractal microstrip antenna for modern wireless co mmunications," *AEU International Journal of Electronics and Co Mmunications*, vol. 123, Article ID 153288, 2020.